РОССИЙСКАЯ АКАДЕМИЯ НАУК

ЖУРНАЛ
ЭКСПЕРИМЕНТАЛЬНОЙ
И ТЕОРЕТИЧЕСКОЙ ФИЗИКИ

ОСНОВАН В МАРТЕ 1873 ГОДА *ТОМ 111, ВЫПУСК 3*
ВЫХОДИТ 12 РАЗ В ГОД *МАРТ, 1997*
МОСКВА «НАУКА»

CONSISTENT TREATMENT OF COLOUR TRANSPARENCY EFFECTS IN DIFFRACTIVE ELECTROPRODUCTION OF VECTOR MESONS OFF NUCLEI

©1997 *O. Benhar*, S. Fantoni**, N. N. Nikolaev***, B. G. Zakharov*****

** INFN Sezione Sanità. Physics Laboratory, Istituto Superiore di Sanità*
Viale Regina Elena, 299. I-00161 Roma, Italy
*** Interdisciplinary Laboratory, SISSA, and INFN, Sezione di Trieste*
Via Beirut, 4, I-34014 Trieste, Italy
**** Institut für Theoretische Kernphysik der Universität Bonn*
Nussallee 14-16, D-53115, Bonn, Germany
***** L. D. Landau Institute for Theoretical Physics*
117940, Moscow, Russia

Submitted 11 July 1996

Nuclear transparency for incoherent real and virtual photoproduction of vector mesons off nuclei depends crucially on the interplay of the initial state and final state interactions. We develop a consistent description of initial state and final state interactions based on the coupled-channel multiple-scattering theory. We present the detailed predictions for incoherent production of the $s\bar{s}$ and $c\bar{c}$ mesons. The onset of initial state interactions is controlled by the production length l_P, and we find strong variations of nuclear transparency when l_P rises with energy and becomes comparable to the radius of the target nucleus R_A. For the $s\bar{s}$ mesons the regime of $l_P \sim R_A$ corresponds to precisely the kinematical range of the HERA-HERMES experiment, whereas for the $c\bar{c}$ mesons the same condition will be met at the electron-nucleus collider ENC at GSI. In spite of the subasymptotic values of Q^2 and ν, we find a complex pattern of colour transparency induced effects whose experimental study may provide information on several issues relevant to the understanding of QCD, both in the perturbative and nonperturbative regimes.

1. INTRODUCTION

The colour transparency (CT) phenomenon in diffractive exclusive virtual photoproduction of vector mesons off nuclear targets has recently attracted much attention [1–8]. The Q^2-dependence of the size of the initial $q\bar{q}$ fluctuation of the virtual photon makes the measurements of the nuclear transparency in these reactions a unique tool for probing the colour-dipole cross section which plays a fundamental role in the low-x physics [9–11]. The measurements of nuclear transparency in vector mesons electroproduction may also give an important information on the spatial wave function of vector mesons [4]. The predictions [4, 5] for CT effects at asymptotic energies have been confirmed in the E665 muon scattering experiment at FERMILAB, although the statistical accuracy of the E665 data was limited [12]. Much more accurate data on nuclear transparency in virtual photoproduction of vector mesons will be obtained in the forthcoming high-luminosity experiments at CEBAF and HERA (HERMES collaboration). In these experiments the energy will be rather low, which makes a thorough theoretical analysis of CT effects at subasymptotic energies a topical issue.

Virtual photons are produced in the scattering of electrons (muons), and nuclear transparency for virtual photoproduction and the photon energy ν and virtuality Q^2 is defined as

$$T_A = \frac{1}{A}\frac{d\sigma(e + A \to e' + A^* + V)}{d\sigma(e + N \to e' + N + V)}, \tag{1}$$

where A is the mass number of the target nucleus. In the incoherent production off the nucleus the nuclear cross section is summed over all the excited and nuclear break-up states A^* excluding production of secondary particles (mesons). In the single incoherent rescattering approximation, the reaction mechanism can be viewed as a formation and propagation of the projectile wave packet, the incoherent (quasi-elastic) scattering of which off the bound nucleon produces the ejectile wave packet which propagates through the nucleus and forms the observed final state vector meson V. The nuclear transparency can be written as

$$T_A(\mathbf{q}) = \frac{1}{A}\int d^3r n_A(\mathbf{r})\frac{|\langle V|\hat{S}_f(\mathbf{r})\hat{f}(\mathbf{q})\hat{S}_i(\mathbf{r})|\gamma^*\rangle|^2}{|\langle V|\hat{f}(\mathbf{q})|\gamma^*\rangle|^2}. \tag{2}$$

Here $n_A(\mathbf{r})$ is the nuclear density, $\mathbf{q}$ is the transverse momentum transfer, $\hat{S}_i(\mathbf{r})$ and $\hat{S}_f(\mathbf{r})$ are the evolution operators describing the coherent initial-state interaction (ISI) of the projectile and final-state interaction (FSI) of the ejectile in a nucleus, respectively, $\hat{f}(\mathbf{q})$ is the scattering matrix which describes the projectile-to-ejectile diffractive transitions in interaction on a free nucleon. The evolution operators $\hat{S}_{i,f}$ and the scattering matrix $\hat{f}$ in Eq. (1) act in a space including both the hadronic states and the photon state. The physical meaning of the numerator in the integrand of (2) is obvious: it is the cross section of the one-fold incoherent interaction with a bound nucleon, modified by the intranuclear coherent ISI of the projectile and FSI of the ejectile, the numerator is the photoproduction cross section on a free nucleon. Equation (1) is valid at $q^2 \lesssim 1/B$, where B is the diffraction slope for photoproduction on a free nucleon, when the many-fold incoherent rescatterings in a nuclear medium can be neglected. For incoherent diffractive scattering of hadrons off nuclei at subasymptotic energies, the counterpart of Eq. (2) has been derived in [13], for the first application to an evaluation of CT effects in the charge exchange of pions off nuclei at asymptotic energies see [14].

To the leading order in the fine-structure constant $\alpha_{em} = 1/137$, the intermediate state decomposition of the matrix element $\langle V|\hat{S}_f(\mathbf{r})\hat{f}(\mathbf{q})\hat{S}_i(\mathbf{r})|\gamma^*\rangle$ which enters Eq. (2) is given by

$$\langle V|\hat{S}_f\hat{f}\hat{S}_i|\gamma^*\rangle = \sum_h \langle V|\hat{S}_f|h\rangle\langle h|\hat{f}|\gamma^*\rangle + \sum_{h,h'}\langle V|\hat{S}_f|h'\rangle\langle h'|\hat{f}|h\rangle\langle h|\hat{S}_i|\gamma^*\rangle\,, \tag{3}$$

where $|h\rangle$, $|h'\rangle$ are the intermediate hadronic states and we have taken into account that to leading order in α_{em} one can set $\langle\gamma^*|\hat{S}_i|\gamma^*\rangle = 1$. The first term in the decomposition (3) describes the incoherent scattering at the level of production of the intermediate state $|h\rangle$ at the electromagnetic interaction vertex and is described by the amplitude $\langle h|\hat{f}|\gamma^*\rangle$. The ISI effects are present only in the second term, in which the incoherent scattering takes place at the level of intermediate states $|h\rangle$ and $|h'\rangle$ and is described by the amplitude $\langle h'|\hat{f}|h\rangle$. The coherency properties of ISI of the projectile and FSI of the ejectile in virtual photoproduction of vector mesons are characterized by the two different length scales. For the ISI the relevant scale is a length of production of the $q\bar{q}$ pair by the virtual photon,

$$l_P \sim \frac{2\nu}{Q^2 + m_V^2}\,, \tag{4}$$

while for the FSI the relevant scale is a length of formation of the wave function, of the final vector meson,

$$l_F \sim \frac{2\nu}{m_{V'}^2 - m_V^2}\,, \tag{5}$$

where $m_{V,V'}$ are the masses of the $1S$ and $2S$ vector mesons [1,2].

The strength of the ISI effects critically depends on the value of the ratio l_P/R_A, where R_A is the nucleus radius. At a sufficiently small energy and/or large Q^2 when $l_P \ll R_A$, the off-diagonal matrix element $\langle h|\hat{S}_i|\gamma^*\rangle$ is suppressed due to the large longitudinal momentum transfer, $\sim 1/l_P$, in the coherent $\gamma^* \to q\bar{q}$ transition. As a result, the second term in Eq. (2) related to the ISI can be neglected. In this case the nuclear effects are exhausted by the FSI, which in its turn depends crucially on the value of the ratio l_F/R_A. In Ref. [2] this regime for $c\bar{c}$ vector meson photoproduction was considered within the Green's function approach to FSI. This technique was further used in Ref. [8] for evaluation of nuclear transparency in $s\bar{s}$ vector meson electroproduction for energy region of the future experiments at CEBAF. At $l_P \gtrsim R_A$ the ISI and FSI must be taken into account on the same footing. In the limit of high energy, when $l_{P,F} \gg R_A$, the ISI and FSI absorption effects can be evaluated within the frozen-size approximation for propagation of the $q\bar{q}$ fluctuation of the virtual photon through nuclear medium [2]. The intermediate energy region when $l_{P,F}$ are comparable with the nucleus size is the most complicated for evaluation of CT effects. In Ref. [3] an approximate formula for nuclear transparency interpolating between the high and low energy regimes was obtained within the two-channel model. For the reason of relatively weak nuclear attenuation in the J/Ψ photoproduction, this interpolation formula works well and the theoretical results of Ref. [3] agree with the experimental data of NMC collaboration [15]. A more rigorous treatment of CT effects at $l_{P,F} \sim R_A$ is highly desirable because the kinematical conditions in the CEBAF and HERA-HERMES experiments on production of light vector mesons correspond precisely to this situation. In the energy range of the electron-nucleus collider ENC which is being planned at GSI, one will encounter the case of $l_P \sim R_A$ in the production of the $J/\Psi, \Psi'$ mesons off

nuclei. (At much higher energies of HERA operating in the electron-nucleus collider mode, one will have the asymptotic situation of $l_P, l_F \gg R_A$, which requires a separate analysis.) The theoretical basis for evaluation of CT effects without restrictions on the values of $l_{P,F}$ is the Glauber–Gribov coupled-channel multiple-scattering theory (CCMST) [16, 17]. The formalism of CCMST allows to take into account both the evolution and absorption effects in propagation of the projectile state through nuclear medium.

The interplay of the ISI and FSI effects is important also in diffractive hadroproduction off nuclei. Because in hadronic interactions one always has $l_P \approx l_F$, the ISI and FSI effects cannot be separated. The virtuality of the photon, Q^2, which can easily be varied experimentally in a broad range, gives an important handle on the values of l_P and the strength of ISI, which makes the real and virtual photoproduction of vector mesons a unique testing ground of the coherency properties of diffractive production off nuclei. In the present paper we perform the CCMST analysis of CT effects in ϕ, ϕ' and J/Ψ, Ψ' electroproduction.

2. THE ISI AND FSI EVOLUTION OPERATORS IN THE COUPLED-CHANNEL MULTIPLE-SCATTERING FORMALISM

We use for evaluation of the ISI and FSI evolution operators $\hat{S}_{i,f}$ an extension of the formalism previously developed [18] for calculation FSI effects in nuclear transparency for quasi-elastic $A(e, e'p)$ scattering. As in the case of the FSI evolution operator for the ejectile state in $(e, e'p)$ scattering, the operators $\hat{S}_i$ and $\hat{S}_f$ within CCMST can be written in z-ordered operator exponential form

$$\hat{S}_i(\mathbf{r}) = \hat{P}_z \exp\left[-\frac{1}{2}\int_{-\infty}^{z} d\xi \hat{\sigma}(\xi - z) n_A(\mathbf{b}, \xi)\right], \tag{6}$$

$$\hat{S}_f(\mathbf{r}) = \hat{P}_z \exp\left[-\frac{1}{2}\int_{z}^{\infty} d\xi \hat{\sigma}(\xi - z) n_A(\mathbf{b}, \xi)\right], \tag{7}$$

where $\mathbf{r} = (\mathbf{b}, z)$, $\hat{P}_z$ is z-ordering operator. The matrix elements of the z-dependent operator $\hat{\sigma}(z)$ are connected with the diffraction scattering matrix at $\mathbf{q} = 0$:

$$\langle i|\hat{\sigma}(z)|j\rangle = -i \exp(ik_{ij}z)\langle i|\hat{f}(\mathbf{q} = 0)|j\rangle, \tag{8}$$

here k_{ij} is the longitudinal momentum transfer related to transition $iN \to jN$ [17],

$$k_{ij} = \frac{m_i^2 - m_j^2}{2\nu}, \tag{9}$$

m_i and m_j are the masses of the states $|i\rangle$ and $|j\rangle$ and for the virtual photon $m_{\gamma^*}^2 = -Q^2$. The exponential phase factor in Eq. (8) results from the difference between the phases for the plane waves describing the states $|i\rangle$ and $|j\rangle$ after propagating the distance z. It is easy to check that the whole phase factors, which the operators (6) and (7) yield in the case of arbitrary sequences of intermediate states for transitions $\gamma^* \to h$ and $h \to V$, coincide with the phase factors which can be obtained by solving the set of the coupled-channel wave equations.

For the numerical calculations it is convenient to treat in (6) and (7) the off-diagonal part of matrix $\hat{\sigma}(z)$ as a perturbation. Then we can represent the matrix elements of the operators $\hat{S}_{i,f}(\mathbf{r})$ in the form of the ν-fold off-diagonal rescatterings series

$$\langle h|\hat{S}_i(\mathbf{r})|\gamma^*\rangle = \sum_{\nu=1}^{\infty}\langle h|\hat{S}_i^{(\nu)}(\mathbf{r})|\gamma^*\rangle\,, \tag{10}$$

$$\langle V|\hat{S}_f(\mathbf{r})|h\rangle = \sum_{\nu=0}^{\infty}\langle V|\hat{S}_f^{(\nu)}(\mathbf{r})|h\rangle\,, \tag{11}$$

where

$$\langle h|\hat{S}_i^{(1)}(\mathbf{b},z)|\gamma^*\rangle = -\frac{1}{2}\sigma_{h\gamma^*}\exp(ik_{\gamma^* h}z)\times$$
$$\times\int_{-\infty}^{z}dz_1 n_A(\mathbf{b},z_1)\exp\left[ik_{h\gamma^*}z_1-\frac{1}{2}t(\mathbf{b},z,z_1)\sigma_{hh}\right], \tag{12}$$

$$\langle h|\hat{S}_i^{(\nu)}(\mathbf{b},z)|\gamma^*\rangle = \left(-\frac{1}{2}\right)^{\nu}\sum_{i_1,\dots i_{\nu-1}}\sigma'_{hi_{\nu-1}}\sigma'_{i_{\nu-1}i_{\nu-2}}\cdots\sigma_{i_1\gamma^*}\exp(ik_{\gamma^* h}z)\times$$
$$\times\int_{-\infty}^{z}dz_\nu n_A(\mathbf{b},z_\nu)\exp\left[ik_{hi_{\nu-1}}z_\nu-\frac{1}{2}t(\mathbf{b},z,z_\nu)\sigma_{hh}\right]\times$$
$$\times\int_{-\infty}^{z_\nu}dz_{\nu-1}n_A(\mathbf{b},z_{\nu-1})\exp\left[ik_{i_{\nu-1}i_{\nu-2}}z_{\nu-1}-\frac{1}{2}t(\mathbf{b},z_\nu,z_{\nu-1})\sigma_{i_{\nu-1}i_{\nu-1}}\right]\dots\times$$
$$\times\int_{-\infty}^{z_2}dz_1 n_A(\mathbf{b},z_1)\exp\left[ik_{i_1\gamma^*}z_1-\frac{1}{2}t(\mathbf{b},z_2,z_1)\sigma_{i_1i_1}\right],\quad \nu\geq 2\,, \tag{13}$$

$$\langle V|\hat{S}_f^{(0)}(\mathbf{b},z)|h\rangle = \delta_{Vh}\exp\left[-\frac{1}{2}t(\mathbf{b},\infty,z)\sigma_{VV}\right], \tag{14}$$

$$\langle V|\hat{S}_f^{(\nu)}(\mathbf{b},z)|h\rangle = \left(-\frac{1}{2}\right)^{\nu}\sum_{i_1,\dots i_{\nu-1}}\sigma'_{Vi_{\nu-1}}\sigma'_{i_{\nu-1}i_{\nu-2}}\cdots\sigma'_{i_1h}\exp(ik_{hV}z)\int_{z}^{\infty}dz_1 n_A(\mathbf{b},z_1)\times$$
$$\times\exp\left[ik_{i_1h}z_1-\frac{1}{2}t(\mathbf{b},z_1,z)\sigma_{hh}\right]\int_{z_1}^{\infty}dz_2 n_A(\mathbf{b},z_2)\exp\left[ik_{i_2i_1}z_2-\frac{1}{2}t(\mathbf{b},z_2,z_1)\sigma_{i_1i_1}\right]\dots\times$$
$$\times\int_{z_{\nu-1}}^{\infty}dz_\nu n_A(\mathbf{b},z_\nu)\exp\left[ik_{Vi_{\nu-1}}z_\nu-\frac{1}{2}t(\mathbf{b},\infty,z_\nu)\sigma_{VV}\right],\quad \nu\geq 1. \tag{15}$$

Here $\sigma'_{ik}=\sigma_{ik}-\delta_{ik}\sigma_{ii}$, the matrix $\hat{\sigma}$ is connected with the forward diffraction scattering matrix, $\hat{f}(\mathbf{q}=0)=i\hat{\sigma}$, and $t(\mathbf{b},z_2,z_1)=\int_{z_1}^{z_2}dz n_A(\mathbf{b},z)$ is the partial optical thickness.

The ISI and FSI evolution operators comprise the two effects: the first can be called the nuclear filtering of the projectile and ejectile wave packets due to the difference of attenuation factors $\exp[-(1/2)t(\mathbf{b}, z_2, z_1)\sigma_{ii}]$, the second is the space-time evolution of these wave packets caused by the off-diagonal coherent rescatterings in a nuclear medium. The first order ISI term $\langle h|\hat{S}_i^{(1)}(\mathbf{b}, z)|\gamma^*\rangle$ of Eq. (12) and zeroth order FSI term $\langle V|S_f^{(0)}(\mathbf{b}, z)|h\rangle$ of Eq. (11) describe the conventional Glauber ISI and FSI absorption, respectively. In this Glauber approximation, only the nuclear filtering effects are included. The terms (13) and (15) give corrections to the ISI and FSI connected with the off-diagonal rescatterings of the intermediate hadronic states in nuclear medium and describe the space-time evolution of the projectile and ejectile wave packets caused by the intranuclear interactions. It is precisely the oscillating exponential phase factors in Eqs. (13) and (15) which lead to a suppression of the contributions of the off-diagonal inelastic intermediate states at low energies of the virtual photon. Notice, that the above discussed suppression of the ISI at $l_P \lesssim R_A$ is also connected with the oscillating exponential phase factor $\exp(ik_{h\gamma^*}z_1)$ in the integrand in Eq. (12). Equations (2), (10)–(15) form the basis for numerical evaluation of nuclear transparency in incoherent vector mesons electroproduction in the framework of CCMST.

3. CALCULATION OF THE DIFFRACTION SCATTERING MATRIX

The ISI and FSI operators $\hat{S}_{i,f}$ describing the evolution of the $q\bar{q}$ state as it propagates through nucleus depend critically on the form of the diffraction matrix. In our analysis we describe the $q\bar{q}$ states in the nonrelativistic oscillator model. Then, assuming the dominance of the Pomeron exchange the diffraction matrix elements σ_{ik} can be written as

$$\langle i|\hat{\sigma}|k\rangle = \int d^2\boldsymbol{\rho}\, dz \Psi_i^*(\boldsymbol{\rho}, z)\sigma(\rho)\Psi_k(\boldsymbol{\rho}, z)\,, \tag{16}$$

where $\boldsymbol{\rho}$ is the transverse size of the $q\bar{q}$ pair, $\Psi_{i,k}(\boldsymbol{\rho}, z)$ are the wave functions describing the $q\bar{q}$ states, and $\sigma(\rho)$ is the dipole cross section describing the interaction of the $q\bar{q}$ pair with a nucleon. We need also the matrix element for the diffraction excitation of the virtual photon into $q\bar{q}$ state on the free nucleon. Following Ref. [2] we use the perturbative $q\bar{q}$ light-cone wave function of the virtual photon [9] and write the matrix elements $\langle i|\hat{\sigma}|\gamma^*\rangle$ in the form

$$\langle i|\hat{\sigma}|\gamma^*\rangle = \lambda \int d^2\boldsymbol{\rho}\, dz \Psi_i^*(\boldsymbol{\rho}, z)\sigma(\rho)K_0(\epsilon\rho)\exp\left(-\frac{z^2}{d^2}\right), \tag{17}$$

where

$$\epsilon^2 = m_q^2 + Q^2/4, \tag{18}$$

m_q is the quark mass, $K_0(x)$ is the modified Bessel function, $d = 1/2m_q$, λ is a normalization coefficient which is immaterial for the evaluation of nuclear transparency. The formula (14) yields the diffraction amplitude for transition of the virtual photon into $q\bar{q}$ state with the sum of quark helicities equal to the photon helicity [2]. This amplitude dominates for production of the nonrelativistic $q\bar{q}$ states and/or for moderately large $Q^2 \lesssim m_V^2$ considered in the present paper.

In our analysis we restrict ourselves to calculation of nuclear transparency at small momentum transfer. Then, we can use Eqs. (16) and (17) for calculation of the scattering matrix

$\hat{f}$ entering the numerator and denominator in the integrand of Eq. (2). At small momentum transfer, rescatterings of the $q\bar{q}$ state on nucleons do not change the projection of its orbital momentum on z-axis. As a result, in the oscillator model the intermediate $q\bar{q}$ states emerging in the coupled-channel formalism are exhausted by the transverse excitations of $q\bar{q}$ system with zero value of the azimuthal quantum number. The masses of these $q\bar{q}$ states entering the formula (9) for longitudinal momentum transfer can be written as $m_i = m_0 + 2i\omega_q$, here ω_q is the oscillator frequency. For the oscillator frequencies of the $s\bar{s}$ and $c\bar{c}$ systems we use the values $\omega_s = (m_{\phi'} - m_\phi)/2 = 0.33$ GeV and $\omega_c = (m_{\Psi'} - m_{J/\Psi})/2 = 0.3$ GeV. For the quark masses we take $m_s = 0.5$ GeV and $m_c = 1.5$ GeV.

The form of the diffraction matrix is sensitive to the ρ-dependence of the dipole cross section. The available experimental data on the structure function F_2 at low x and the cross sections of vector meson electroproduction off nucleon can be described by representing the dipole cross section as a sum of the energy dependent perturbative and the energy independent nonperturbative components [11]. The energy dependence of the perturbative part of $\sigma(\rho)$ generated by the higher Fock-states is governed by the generalized BFKL equation [19]. The analysis of CT effects at high energy in the regime of large contribution to the dipole cross section of higher Fock-states requires an accurate treatment of the nuclear filtering effects for the many-body parton components of the projectile and ejectile. The interplay of the absorption effects for the different Fock-states may be important for energy dependence of nuclear transparency in the limit $l_P \gg R_A$. In the present paper we restrict ourselves to evaluation of CT effects at relatively small energies when the higher Fock-states do not affect considerably nuclear transparency. We use for $\sigma(\rho)$ the parameterization given by the two-gluon exchange model of the pomeron [20, 21] which gives the energy independent dipole cross-section

$$\sigma(\rho) = \frac{16}{3}\int d^2\mathbf{k}\,\frac{\alpha_S(\max(C/\rho,k))\alpha_S(k)\,[1-\exp(i\mathbf{k}\boldsymbol{\rho})]\,[1-G_2(\mathbf{k},-\mathbf{k})]}{(k^2+\mu_g)^2}, \qquad (19)$$

here $G_2(\mathbf{k}_1,\mathbf{k}_2) = \langle N|\exp(i\mathbf{k}_1\mathbf{r}_1 + i\mathbf{k}_2\mathbf{r}_2)|N\rangle$ is the two-quark formfactor of the nucleon, μ_g is an effective gluon mass, and $C \simeq 1.5$ [9]. We calculated the dipole cross section making use of the running and freezing coupling $\alpha_S(k)$ according to the prescription of Ref. [9]. The value of α_S was frozen at the momenta $k \le k_{fr} = 0.7$ GeV. At higher momenta the running α_S was calculated through the one-loop formula with $\Lambda_{QCD} = 0.3$. As in Ref. [22], we use for the effective gluon mass value $\mu_g = 0.17$ GeV. The ρ-dependence of the dipole cross section calculated within the two-gluon model is shown in Fig. 1. Calculation of $\sigma_{tot}(\pi N) = \langle\pi|\hat{\sigma}|\pi\rangle$ with our parameterization of the dipole cross section reproduces the experimental value of the pion-nucleon total cross section in the ten-hundred GeV's energy region.

The decrease of the dipole cross section $\sigma(\rho)$ at perturbatively small ρ given by the parameterization (19) agrees well with the behavior of the dipole cross section extracted recently from the experimental data on the vector mesons electroproduction off the free nucleon for the range of dipole size $\rho \sim 0.2$–1.5 fm [23]. The ρ-dependence of the dipole cross section given by Eq. (19) was previously corroborated by the results of analysis of CT effects in quasi-elastic charge exchange reaction $\pi^- A \to \pi^0 A'$ [14] and of the nuclear shadowing and diffraction cross section in deep inelastic scattering [9, 24].

At this point, it must be made clear that the above choice of the gluon mass is oriented towards description of the nonperturbative part of the dipole cross section and μ_g is a phenomenological parameter which must not be taken at the face value. The analysis of low-x HERA data on the structure function F_2 [11] within the generalized BFKL equation [19], and the nonperturbative evaluation of the gluon correlation radius [25] yield a clearcut evidence

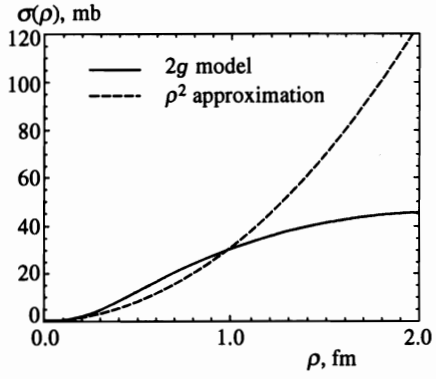

Fig. 1. The dipole-size dependence of colour dipole cross sections of parameterizations (19) (the solid line) and (21) (the dashed line)

in favour of the effective gluon mass ~ 0.75 GeV. The value of μ_g used in the present paper does not affect the dipole cross section at perturbatively small $\rho \ll 1/\mu_g$, but it provides a viable parameterization of the experimental information on the dipole cross section in the semiperturbative and nonperturbative regions of larger ρ, which really cannot be described in the perturbative QCD.

Making use of the parameterization (19) for $\sigma(\rho)$, with the above set of the quark masses and the oscillator frequencies we find the following total cross sections of interaction of the vector mesons with the free nucleon: $\sigma_{tot}(\phi N) \approx 16$ mb, $\sigma_{tot}(\phi' N) \approx 24.5$ mb, $\sigma_{tot}(J/\Psi N) \approx 7.5$ mb and $\sigma_{tot}(\Psi' N) \approx 14.5$ mb. For the ratio $\langle V(2S)|\hat{\sigma}|\gamma^*\rangle/\langle V(1S)|\hat{\sigma}|\gamma^*\rangle$ at $Q^2 = 0$ we obtain the values 0.186 and 0.49 for the $s\bar{s}$ and $c\bar{c}$ mesons, respectively. Notice that the resulting ratio $R(2S/1S) = \sigma(\gamma^* N \to \Psi' N)/\sigma(\gamma^* N \to J/\Psi N) \approx 0.24$ predicted for $Q^2 = 0$ agrees well with the result of the NMC collaboration $R(2S/1S) = 0.22 \pm 0.05$ [26] and $R(2S/1S) = 0.21 \pm 0.02$ from the E687 collaboration [27].

In conclusion of this section it is appropriate to discuss the scanning phenomenon and the effect of the nodal structure of the spatial wave function of radially excited $2S$ vector mesons on the amplitude of the transition $\gamma^* \to V(2S)$. The transverse spatial $q\bar{q}$ wave function of the virtual photon, $\propto K_0(\epsilon\rho)$, which enters the matrix element (17), decreases proportionally to $\exp(-\epsilon\rho)$ at large $\rho \gtrsim 1/\epsilon \sim 1/\sqrt{m_q^2 + Q^2/4}$, see Eq. (19). Due to the vanishing of the dipole cross section at $\rho = 0$, the typical size of the $q\bar{q}$ pair dominating in the matrix element (17), so called scanning radius r_S [4], turns out to be considerably greater than the naively expected value $\sim 1/\sqrt{m_q^2 + Q^2/4}$ and is given by

$$r_S \approx \frac{6}{\sqrt{Q^2 + m_V^2}} \tag{20}$$

(here we put $2m_q \approx m_V$). At low Q^2 the value of r_S is close to the radius r_V of the $1S$ state and to the position of the node, $r_n \sim r_V$, in the spatial wave function of the radially excited $2S$ vector mesons. This leads to a considerable cancellation between the contributions to the amplitude $\langle V(2S)|\hat{\sigma}|\gamma^*\rangle$ coming from the regions of large, $\rho \gtrsim r_n$, and small $\rho \lesssim r_n$, dipole size [3, 28]. Precisely this cancellation is responsible for the above cited suppression of the cross section of photoproduction of $2S$ vector mesons as compared to $1S$ vector mesons. Similar suppression of the production amplitude $\langle V(nS)|\hat{\sigma}|\gamma^*\rangle$ holds for higher states $V(nS)$. The

effect is extremely strong for light vector mesons. For the diffraction amplitudes $\langle V(2S)|\hat{\sigma}|\gamma^*\rangle$ for light vector mesons and at low Q^2, one may have either the undercompensation scenario with dominance of the small ρ contribution, or the overcompensation scenario with dominance of the large ρ contribution. Which scenario is realized can only be decided experimentally. To this end, the nuclear filtering effects affect drastically the cancellation between the contributions of the regions of large and small interquark distances to the $2S$ vector meson photoproduction amplitudes. The analysis of ρ' photoproduction in the frozen-size approximation appropriate in the high energy regime performed in Ref. [6] shows that the strong nodal effect for light $2S$ vector mesons can lead to an anomalous A-dependence of nuclear transparency. The behaviour of nuclear transparency for light $2S$ vector mesons at low Q^2 differs strongly for undercompensation and overcompensation scenarios. Within our model for the dipole cross section and for the wave functions of vector mesons, the undercompensation regime takes place in real photoproduction of the ϕ' and Ψ' on the free nucleon at $Q^2 = 0$. In contrast to Ψ', for the ϕ' the compensation effect is very strong and at present the overcompensation regime for ϕ' photoproduction also cannot be excluded. The recent analysis [23] of vector meson photoproduction on free nucleon within the light-cone wave function formalism shows that for photoproduction of light $2S$ vector mesons by the longitudinal photons the relativistic effects can lead to the overcompensation scenario at low Q^2. In order to illustrate the behaviour of nuclear transparency in the overcompensation scenario, we also compute nuclear transparency making for the parameterization of $\sigma(\rho)$ in the form

$$\sigma(\rho) = \rho^2 \frac{\sigma_{tot}(\phi N)}{\langle\phi|\rho^2|\phi\rangle}, \tag{21}$$

which enhances the large ρ contribution and leads to the overcompensation scenario for ϕ' photoproduction, although this parameterization is somewhat unrealistic in view of the available experimental information on the dipole cross section $\sigma(\rho)$ analyzed in [23]. The normalization in (21) has been so chosen as to have approximately the same results for $T(\phi)$, while emphasizing the overcompensation effects in $T(\phi')$.

4. NUMERICAL RESULTS

We performed our numerical calculations for the region $Q^2 \lesssim 2m_V^2$. The number of the included resonance $q\bar{q}$ states and the multiplicity of the off-diagonal rescatterings used in Eqs. (7)–(12) were equal to 5 and 3, respectively. We checked that the contributions from higher excitations and rescatterings with $\nu > 3$ are negligible in the above region of Q^2 even at high energies when the suppression of the higher mass states related to the longitudinal momentum transfer vanishes. The fact that in the above region of Q^2 predictions of the CCMST are saturated by the contribution of several lowest resonance $q\bar{q}$ states has two connected reasons: the suppression of the diffraction matrix element (16) for transitions with large difference between the masses of the initial and final states, and the similar suppression of matrix elements (17) for virtual photoexcitation of higher states $|h\rangle$ for the relatively large value of the scanning radius (20).

In the present paper we focus on predictions for nuclear transparency in ϕ, ϕ', J/Ψ and Ψ' virtual photoproduction on the target nuclei ^{9}Be, ^{56}Fe and ^{207}Pb. For the nuclear matter density in the target nucleus ^{9}Be we use the oscillator shell model nuclear density with the oscillator frequency adjusted to reproduce the experimental value of the root-mean-square radius of the

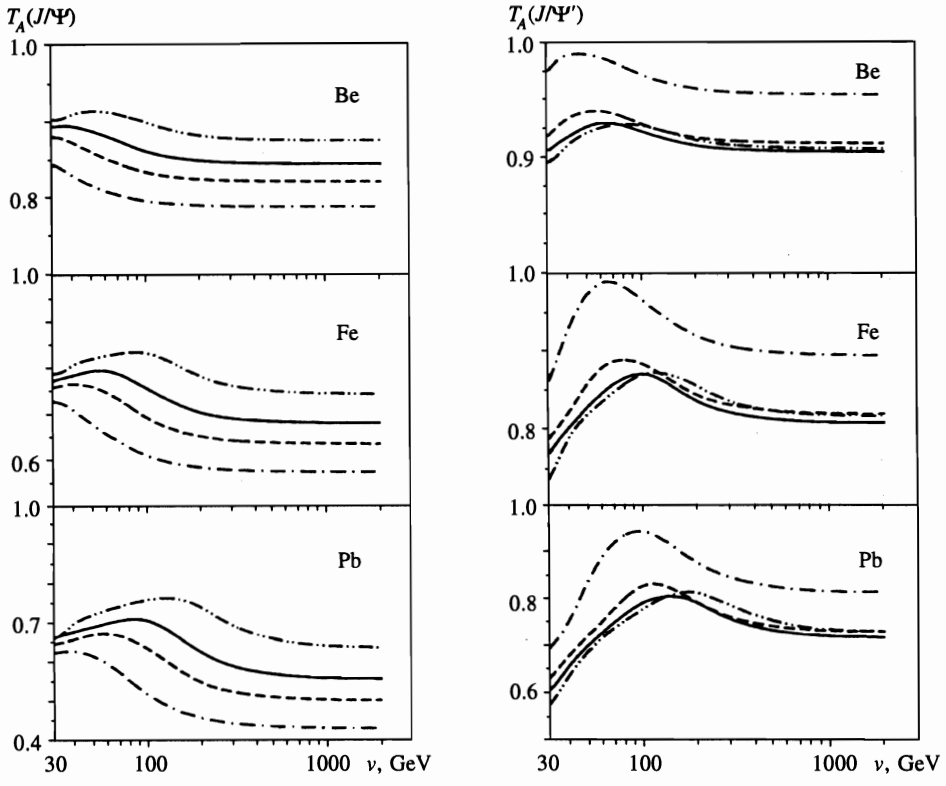

Fig. 2. Predictions for nuclear transparency in incoherent production of the $J/\Psi(1S)$ and $\Psi'(2S)$ mesons off nuclei for the colour dipole cross section of Eq. (19). The dot-dashed, dashed, solid and dot-dot-dashed curves are for Q^2 =0, 5, 10 and 20 GeV^2, respectively

charge distribution $\langle r^2\rangle^{1/2}_{^9\mathrm{Be}} = 2.51$ fm [29]. For the target nucleus ^{56}Fe the parameterization of the nuclear density through a sum of Gaussians from Ref. [29] was used. For ^{207}Pb the Wood-Saxon parameterization of the nuclear density with parameters borrowed from [29] was used.

The results obtained for the dipole cross section parameterized by Eq. (19) are shown in Figs. 2 and 3. At low energies, the magnitude of nuclear transparencies $T_A(\phi)$ and $T_A(J/\Psi)$ is controlled by FSI attenuation of the ejectile. The decrease of $T_A(\phi)$ and $T_A(J/\Psi)$ towards higher energies is due to the onset of attenuation for the ISI effects. The energy ν at which $T_A(\phi)$ and $T_A(J/\Psi)$ start dropping is higher for larger Q^2 and for heavier vector mesons, which nicely correlates with the condition $l_P \gtrsim R_A$, i.e., $\nu \gtrsim R_A(m_V^2 + Q^2)$ for the fully developed ISI. This ISI driven drop of nuclear transparency is preceded by a rise of $T_A(\phi)$ and $T_A(J/\Psi)$ at lower energies. We shall comment more on the origin of this rise below, when discussing the results for the Glauber approximation to the ISI and FSI operators shown below in Figs. 6 and 7. The asymptotic values of $T_A(\phi)$ and $T_A(J/\Psi)$ rise with Q^2 which is the CT effect. In the frozen size approximation, appropriate at high energies, this diminishing attenuation derives from the decrease of the scanning radius r_S with Q^2, see Eq. (20).

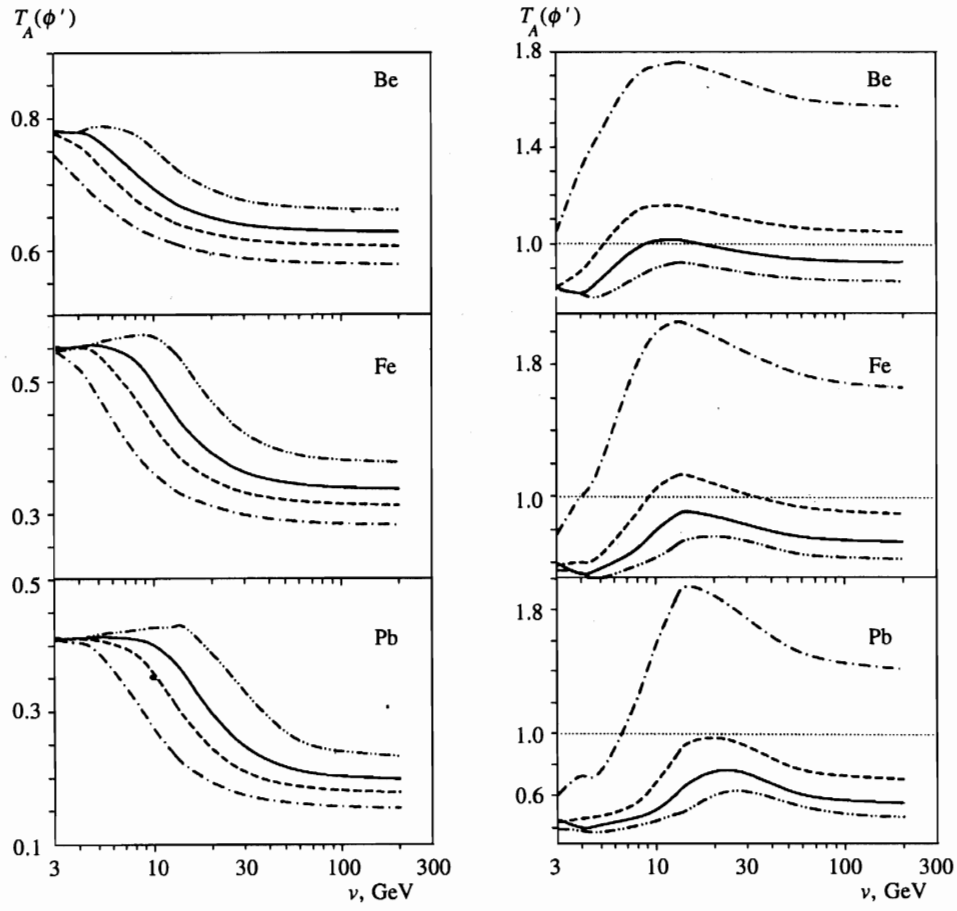

Fig. 3. Predictions for nuclear transparency in incoherent production of the $\phi(1S)$ and $\phi'(2S)$ mesons off nuclei for the colour dipole cross section of Eq. (19). The dot-dashed, dashed, solid and dot-dot-dashed curves are for $Q^2 = 0, 0.5, 1.0$ and 2.0 GeV^2, respectively

The preasymptotic rise of nuclear transparency is much stronger for the $2S$ vector mesons. Also for the $2S$ states the onset of ISI is followed by the decrease of $T_A(\phi')$ and $T_A(\Psi')$ towards higher energies. At small Q^2, when the scanning radius r_S is larger and the node effect is stronger, both $T_A(\phi')$ and $T_A(\Psi')$ exhibit rapid Q^2-dependence, faster than for $T_A(\phi)$ and $T_A(J/\Psi)$, respectively. At much higher Q^2, when the scanning radius r_S is substantially smaller than the radius r_V of the $1S$ states, the role of the node effect diminishes and we shall find $T_A(\phi') \approx T_A(\phi)$ and $T_A(\Psi') \approx T_A(J/\Psi)$ (for more discussion on this point see [4]). Nuclear transparency for the $2S$ states reaches the maximum value in the regions $\nu \sim$ 10–30 GeV for ϕ' photoproduction and $\nu \sim$ 50–150 GeV for Ψ' photoproduction. Our results show that despite the inequality $\sigma_{tot}(V'N) > \sigma_{tot}(VN)$, in the kinematical region studied the counterintuitive inequality $T_A(V(2S)) > T_A(V(1S))$ is predicted. For real ϕ' photoproduction ($Q^2 = 0$) we predict a considerable antishadowing effect. Of course, one must bear in mind that due to the above discussed strong node effect in the ϕ' photoproduction the theoretical predictions for $T_A(\phi')$ at low Q^2 are very model-dependent. We consider the above predictions for nuclear

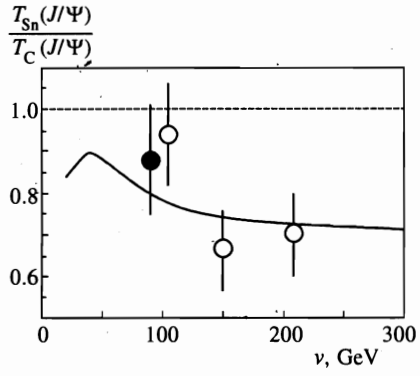

Fig. 4. Predictions for the ratio of nuclear transparencies in incoherent photoproduction of the J/Ψ off Sn and C targets for the dipole cross section of Eq. (19) in comparison with the experimental data from the NMC muon scattering experiment. The open and full circles are for the muon energy 280 GeV and 200 GeV, respectively [15]

transparency for the ϕ' photoproduction only as an illustration of the energy and Q^2-dependence of nuclear transparency expected for the undercompensation scenario. Notice that much of the interesting energy dependence of $T_A(\phi)$ and $T_A(\phi')$ takes place at energies $\nu \sim$ 10–30 GeV, which is precisely the kinematical range of the HERA-HERMES experiment. Similarly, the interesting variations of $T_A(J/\Psi)$ and $T_A(\Psi')$ takes place at energies $\nu \sim$ 30–200 GeV, which are in the kinematic range of the ENC collider.

In Fig. 4 we compare the theoretical predictions obtained for the dipole cross section (19) with the experimental data on the ratio of nuclear transparencies for tin and carbon targets at $Q^2 = 0$ from the NMC collaboration [15]. The agreement between theory and experiment is good. Here we would like to note that in the case of the energy dependence of the ratio $T_{Sn}(J/\Psi)/T_C(J/\Psi)$, the results obtained within the full CCMST turn out to be very close to the evaluation of the energy dependence from the approximate two-channel extrapolation formula for nuclear transparency suggested in [3].

In Figs. 5 and 6 we show the nuclear transparency obtained with the quadratic parameterization of the dipole cross section (21). As was stated above, this parameterization was so devised as to enforce the overcompensation scenario and to have the negative amplitude for $\gamma^* \to \phi'$ transition at low Q^2. For the Ψ' production the undercompensation regime is retained. In the undercompensaiton scenario, nuclear transparency $T_A(\phi')$ decreases monotonously in the considered range of Q^2. In the overcompensation scenario $T_A(\phi')$ rises with Q^2 at low Q^2, which is mostly due to the decrease of the denominator in Eq. (2) with rising Q^2. In our simplified model in which we neglect the small real part of the pomeron amplitudes, $T_A(\phi')$ even becomes infinite at a certain value of Q^2 at which the denominator in Eq. (2) vanishes and then decreases with Q^2 following the pattern for the undercompensation regime. In a more realistic model, the infinity of $T_A(\phi')$ is removed and one will rather find a maximum in $T_A(\phi')$ if one takes into account the nonzero real part of the amplitude for $\gamma^* \to \phi'$ transition. We shall not dwell on that and only wish to emphasize, that an experimental observation of such a nonmonotonous Q^2-dependence of $T_A(\phi')$ will be a clearcut evidence for the overcompensation scenario in ϕ' electroproduction. For the $1S$ states, we find only marginal changes of $T_A(J/\Psi)$ and $T_A(\phi)$ from the ones shown in Figs. 3 and 4 for the dipole cross section (19). For the J/Ψ, Fig. 5 shows an attenuation weaker than in Fig. 3 slightly, which is obvious from the fact that the dipole cross section (21) is smaller than the parameterization (19) in the region of ρ relevant for the J/Ψ production. The cross sections (19) and (21) differ substantially only at $\rho \gtrsim 1$ fm and the changes of $T_A(\Psi')$ from one parameterization to another are also marginal.

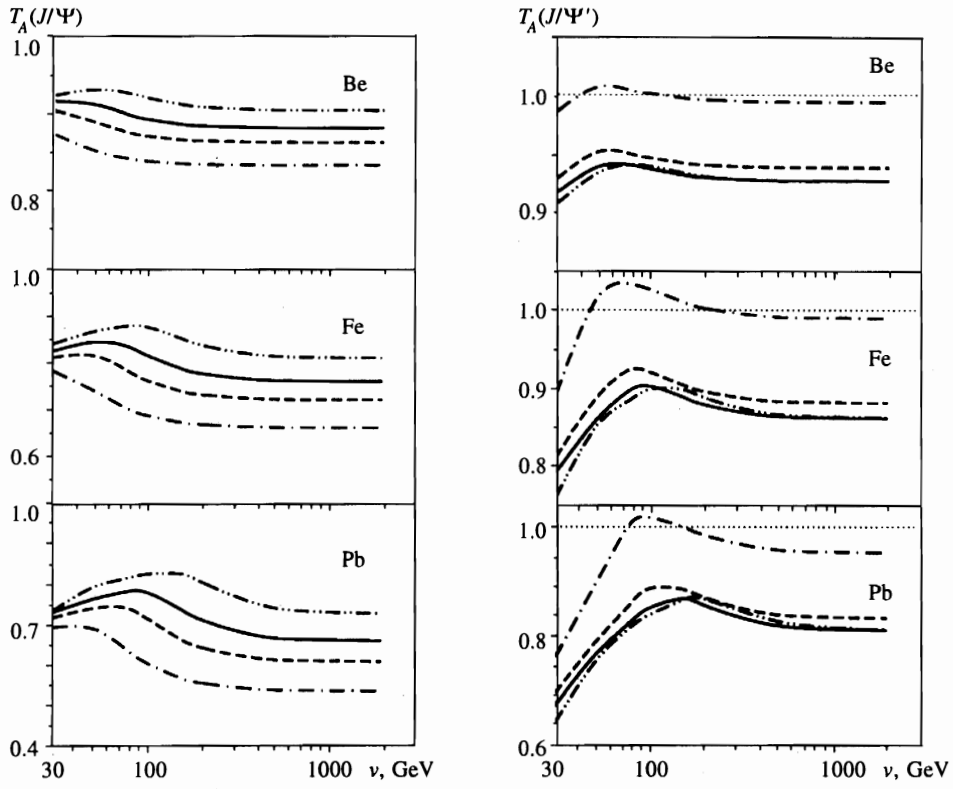

Fig. 5. The same as Fig. 2, but for the dipole cross section of Eq. (21)

The node effect is somewhat enhanced, though, and the inequality $T_A(\Psi') > T_A(J/\Psi)$ becomes stronger, with $T_A(\Psi')$ even reaching the antishadowing regime of $T_A(\Psi')$ for $Q^2 \sim 0$. Finally, the CT effect derives from the variation of $\sigma(\rho)$ with ρ. Because this variation is stronger for the parameterization (21), the Q^2-dependence of $T_A(J/\Psi)$ and $T_A(\phi)$ in the high-energy regime of developed ISI is somewhat stronger for the parameterization (21) than for the parameterization (19), in particular for the $T_A(\phi)$, cf. Fig. 6 and Fig. 3.

The rise of $T_A(J/\Psi)$ and $T_A(\phi)$ with Q^2 is the CT effect, which in the framework of CCMST derives from the off-diagonal transitions $h \to h' \to ... \to V$ and in the ISI and FSI operators and from the interference of transitions $\gamma^* \to V$ and $\gamma^* \to h$ in the photoabsorption vertex. It is interesting to assess the relative importance of different off-diagonal transitions. In the most naive and unrealistic single-channel vector meson dominance (VMD) model one allows only the $\gamma^* \to V$ transitions in the photoabsorption vertex and the diagonal $V \to V$ transitions in the ISI and FSI operators. The energy dependence caused by the onset of ISI is present even in VMD, but it completely fails to describe the Q^2-dependence of photoproduction on the free nucleons, all the CT effects are lost, and we skip a discussion of this unrealistic approximation. A more interesting case is when the ISI and FSI operators are approximated by

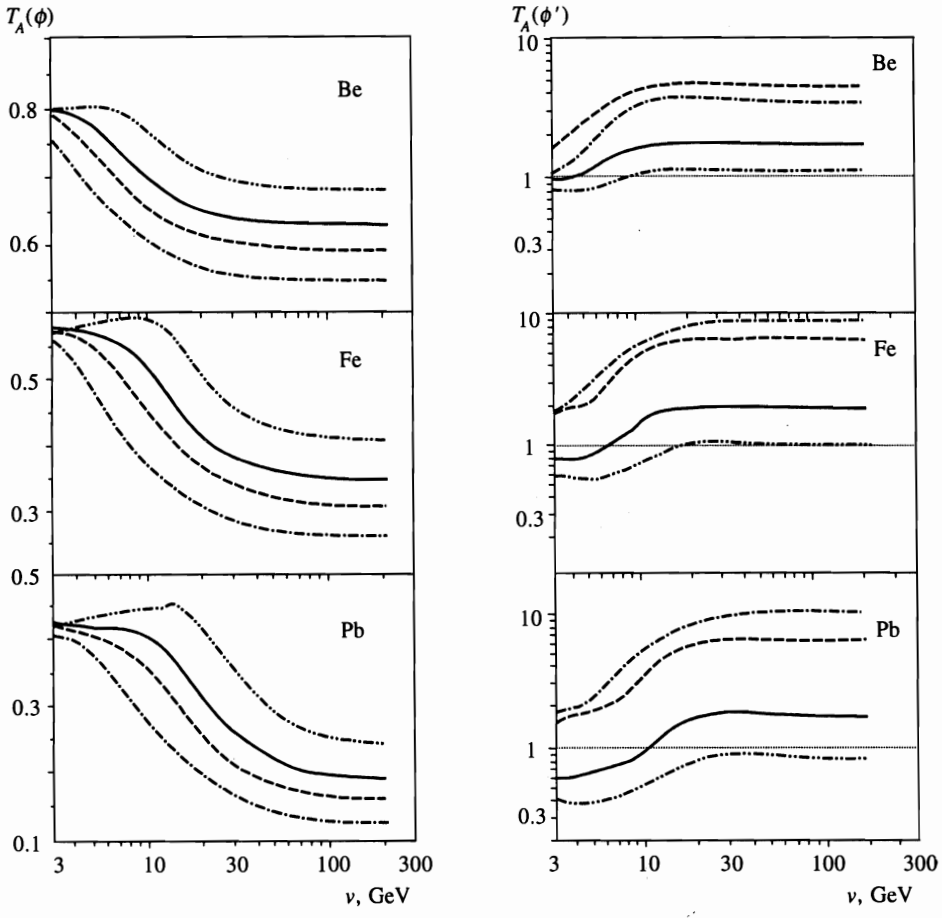

Fig. 6. The same as Fig. 3, but for the dipole cross section of Eq. (21)

the Glauber formulas (12) and (14). In such a simplified model, which we dub here the Glauber approximation, one neglects the evolution of the ejectile and projectile wave packets caused by the off-diagonal rescatterings. The retention of the interference of transitions $\gamma^* \to V$ and $\gamma^* \to h$ in the photoabsorption vertex gives the Q^2-dependent projectile wave packet and the interference of the diagonal $V \to V$ and of the off-diagonal $h \to V$ transitions in the incoherent rescattering vertex allow a correct description of the Q^2-dependence of the free nucleon cross section. The importance of off-diagonal transitions in the FSI operator is best seen from the comparison of the energy dependence of $T_A(J/\Psi)$ in Figs. 3 and 7 and of $T_A(\phi)$ in Figs. 4 and 8 in the low-energy regime of $l_P \lesssim R_A$. In Figs. 7 and 8 nuclear transparency is flat versus energy ν, whereas in Figs. 3 and 4 nuclear transparency exhibits a growth, which is a contribution from the off-diagonal transitions to the CT effect. For the same reason, the Q^2-dependence of $T_A(V(1S))$ in the regime of developed ISI at high energies is weaker in the Glauber approximation, cf. Figs. 7, 8 and Figs. 3, 4, which is an evidence for importance of the off-diagonal transitions also in the ISI. The difference between the full CCMST and Glauber approximation is even stronger in the case of the $2S$ states. Here the Glauber model

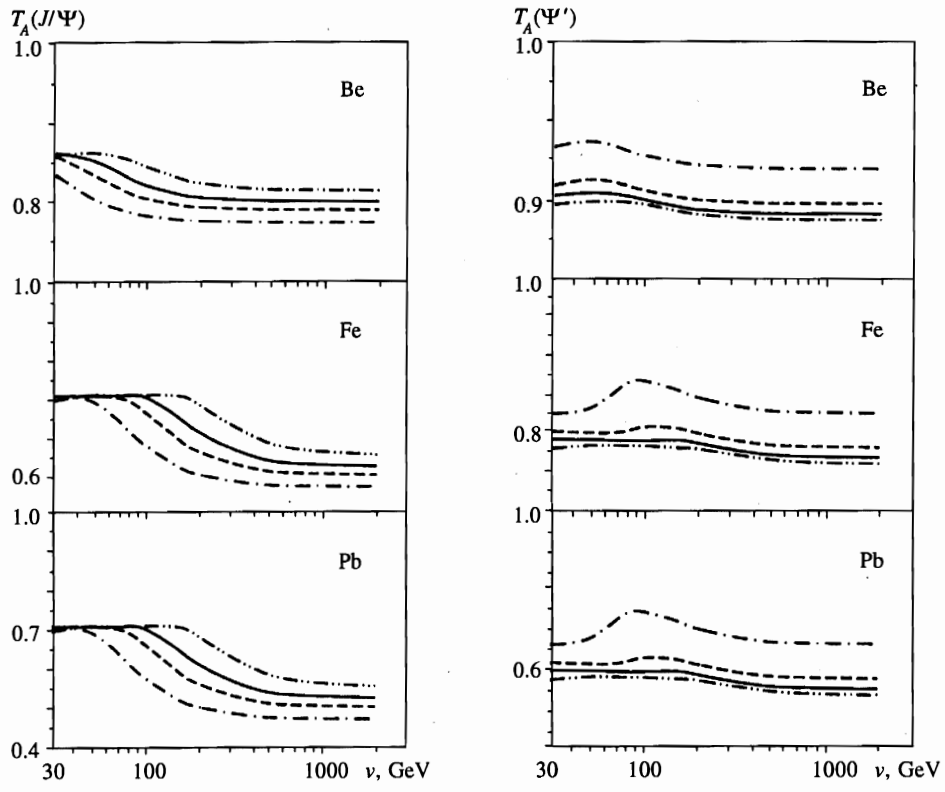

Fig. 7. The same as Fig. 2, but in the Glauber approximation as described in the text. The dipole cross section of Eq. (19) is used

substantially underestimates the CT effects, most notably the preasymptotic growth of $T_A(\Psi')$ with energy and the Q^2-dependence at high energies.

The high-energy region where the curves presented in Figs. 2 and 3 become flat corresponds to the regime when the transverse interquark distance is frozen during propagation of the $q\bar{q}$ fluctuation of the virtual photon through target nucleus. At the same time this is the regime of the developed ISI. In order to illustrate the energy dependence of the strength of ISI, in Fig. 9 we show the ratio of nuclear transparency obtained with the ISI excluded, i.e., putting $\langle h|\hat{S}_i|\gamma^*\rangle = 0$ in the decomposition (3), to nuclear transparency computed with full allowance for both ISI and FSI. As one can see, neglecting the ISI leads to a systematic overestimate of nuclear transparency for $1S$ states. For $2S$ vector mesons a more complicated interplay of the ISI and FSI effects takes place at lower energies. After the energy upgrade, the virtual photon energy $\nu \sim$ 5–8 GeV will become feasible in experiments at CEBAF. Fig. 9 shows that evaluations of $T_A(\phi)$ and $T_A(\phi')$ carried out in [8] neglecting the ISI have the accuracy about 20–30%. The interpretation of the higher energy data from the HERA-HERMES experiment requires the full allowance for ISI. Still another slight difference between

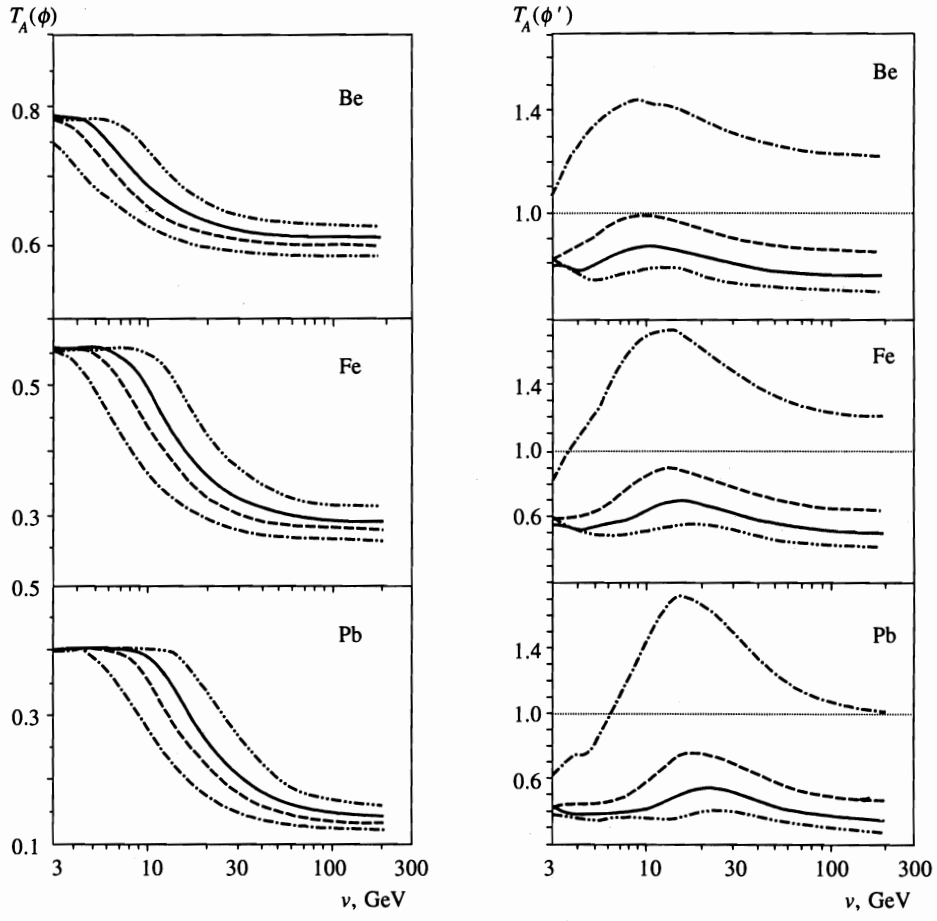

Fig. 8. The same as Fig. 3, but in the Glauber approximation as described in the text. The dipole cross section of Eq. (19) has been used

the present calculations and those in Ref. [8] is in the parameterization of the dipole cross section. In [8] we parameterized the dipole cross section as $\sigma(\rho) = \sigma_0 \left[1 - \exp\left(-\rho^2/R_0^2\right)\right]$, which reproduces well the gross features of the cross section of the model of Eq. (19).

5. CONCLUSIONS

We presented a consistent theory of coherency effects in initial and final state interaction effects for virtual photoproduction of vector mesons off nuclei. The relative role of nuclear filtering and of the off-diagonal coherent rescatterings in the ISI and FSI for the onset of colour transparency effects is elucidated. The onset of ISI with the increasing energy of the photon is shown to have a very strong impact on nuclear transparency and on the onset of colour transparency effects. For the light vector mesons, the onset of ISI takes place in the kinematical domain of the HERA-HERMES experiment, for the charmonium states the interesting energy dependence of nuclear transparency takes place in the kinematical domain of the GSI-ENC.

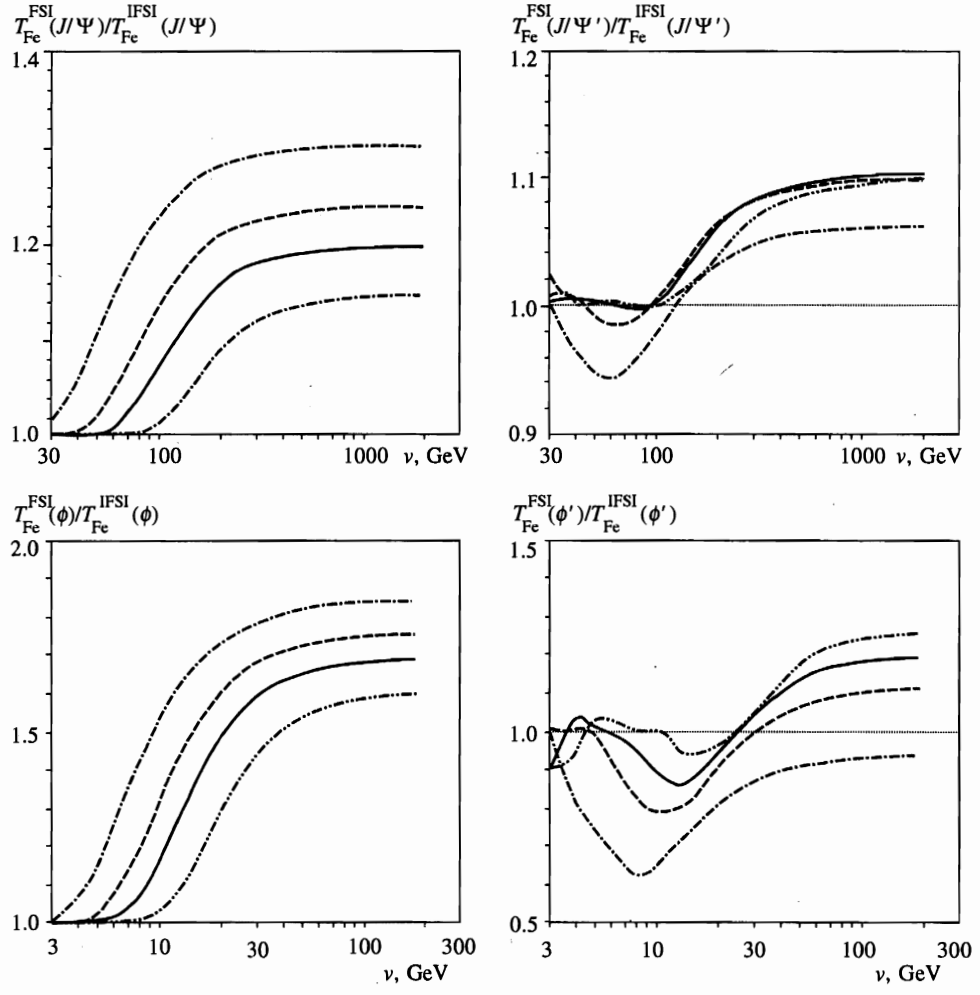

Fig. 9. The ratio of nuclear transparencies for incoherent production of the J/Ψ, Ψ', ϕ, and ϕ' mesons off nuclei evaluated including only final state interaction and neglecting the initial state interaction (FSI), and with the both initial and final state interactions included (IFSI). The legend of curves for J/Ψ and Ψ' mesons is the same as in Fig. 2 and for ϕ and ϕ' mesons as in Fig. 3. The dipole cross section of Eq. (19) has been used

B. G. Z. and N. N. N. thank Prof. J. Spetch for the hospitality at IKP, KFA Juelich, where this work was partly done. The work of N. N. N. was supported by the DFG grant ME864/132-1. N. N. N. is grateful to Prof. U. Meissner for the hospitality at ITKP, University of Bonn.

References

1. S. J. Brodsky and A. H. Mueller, Phys. Lett. B **206**, 685 (1988).
2. B. Z. Kopeliovich and B. G. Zakharov, Phys. Rev. D **44**, 3466 (1991).
3. O. Benhar, B. Z. Kopeliovich, C. Mariotti et al., Phys. Rev. Lett. **69**, 1156 (1992).
4. B. Z. Kopeliovich, J. Nemchick, N. N. Nikolaev, and B. G. Zakharov, Phys. Lett. B **309**, 179 (1993).
5. B. Z. Kopeliovich, J. Nemchick, N. N. Nikolaev, and B. G. Zakharov, Phys. Lett. B **324**, 469 (1994).
6. J. Nemchick, N. N. Nikolaev, and B.G. Zakharov, Phys. Lett. B **339**, 194 (1994).
7. S. J. Brodsky, L. Frankfurt, J. F. Gunion et al., Phys. Rev. D **50**, 3134 (1994).
8. O. Benhar, B. G. Zakharov, S. Fantoni, and N. N. Nikolaev, Phys. Rev. Lett. **74**, 3565 (1995).
9. N. N. Nikolaev and B. G. Zakharov, Z. Phys. C **49**, 607 (1991).
10. N. N. Nikolaev and B. G. Zakharov, Z. Phys. C **64**, 631 (1994).
11. N. N. Nikolaev and B. G. Zakharov, Phys. Lett. B **327**, 149 (1994).
12. E665 Collaboration: M. R. Adams, S. Aid, P. L. Anthony et al., Phys. Rev. Lett. **74**, 1525 (1995).
13. N. N. Nikolaev, Zh. Exp. Teor. Phys. **81**, 814 (1981). Engl. transl: Sov. Phys. JETP **54**, 434 (1981).
14. B. Z. Kopeliovich and B. G. Zakharov, Sov. J. Nucl. Phys. **46**, 911 (1987); Phys. Lett. B **264**, 434 (1991).
15. NMC Collaboration: M. Arneodo, A. Arvidson, B. Badelek et al., Phys. Lett. B **332**, 195 (1994).
16. R. J. Glauber, in: *Lectures in Theoretical Physics*, Vol. 1, ed. by W. Brittain and L. G. Dunham, Interscience Publ., New York (1959); R. J. Glauber and G. Matthiae, Nucl. Phys. B **21**, 135 (1970).
17. V. N. Gribov, Sov. Phys. JETP **29**, 483 (1969); **30**, 709 (1970).
18. O. Benhar, S. Fantoni, N. N. Nikolaev, J. Spetch, A. Usmani, and B. G. Zakharov, Zh. Exp. Teor. Fiz. **110**, 1933 (1996).
19. N. N. Nikolaev, V. R. Zoller, and B. G. Zakharov, Phys. Lett. B **328**, 143 (1994).
20. F. E. Low, Phys. Rev. D **12**, 163 (1975).
21. J. F. Gunion and D. E. Soper, Phys. Rev. D **15**, 2617 (1977).
22. B. G. Zakharov, Sov. J. Nucl. Phys. **49**, 860 (1989).
23. J. Nemchik, N. N. Nikolaev, E. Predazzi, and B. G. Zakharov, Phys. Lett. B **374**, 199 (1996).
24. N. N. Nikolaev and B. G. Zakharov, Z. Phys. C **53**, 331 (1992).
25. E. Schuryak, Rev. Mod. Phys. **65**, 1 (1993).
26. NMC Collaboration: P. Amaudruz, M. Arneodo, A. Ervidson et al., Nucl. Phys. B **371**, 553 (1992).
27. E687 Collaboration: P. L. Frabetti, H. W. K. Cheung, I. P. Cumalat et al., Report at the Europhysics Conference on High Energy Physics, Brussels, June 1995.
28. N. N. Nikolaev, Comments Nucl. Part. Phys. **21**, 41 (1992).
29. H. de Vries, C. W. de Jaeger, and C. de Vries, Atomic Data and Nuclear Data Tables **36**, 496 (1987).